Scientific Research Publishing

Advances in Materials Physics and Chemistry, 2025, 15(5), 75-89
https://www.scirp.org/journal/ampc
ISSN Online: 2162-5328
ISSN Print: 2162-531X

Calculation and Analysis of the Thermodynamic Properties of Air-Aerosols Mixtures

Wepari Charles Yaguibou[1*], Aly Rachid Korbeogo[2], Ibrahim Pafadnam[3], Niessan Kohio[4], Abdoul Karim Kagone[5], Zacharie Koalaga[5]

[1]Centre Universitaire de Dori, Université Thomas Sankara, Ouagadougou, Burkina Faso
[2]Ecole Polytechnique de Ouagadougou, Ouagadougou, Burkina Faso
[3]UFR Science et Technologie, Université Thomas Sankara, Ouagadougou, Burkina Faso
[4]Ecole Normale Supérieure, Ouagadougou, Burkina Faso
[5]UFR Science et Technologie, Université Joseph Ki-Zerbo, Ouagadougou, Burkina Faso
Email: *weparicharles@gmail.com

How to cite this paper: Yaguibou, W.C., Korbeogo, A.R., Pafadnam, I., Kohio, N., Kagone, A.K. and Koalaga, Z. (2025) Calculation and Analysis of the Thermodynamic Properties of Air-Aerosols Mixtures. *Advances in Materials Physics and Chemistry*, **15**, 75-89.
https://doi.org/10.4236/ampc.2025.155005

Received: March 21, 2025
Accepted: May 27, 2025
Published: May 30, 2025

Abstract

Circuit breakers and other electrical equipment are often exposed to operational challenges caused by dust contamination, particularly short-circuit failures. These issues are frequently linked to the deposition of aerosols containing compounds such as aluminium oxide (Al_2O_3), calcium oxide (CaO), iron oxide (Fe_2O_3), and silicon dioxide (SiO_2) on critical components. While previous research has examined the influence of individual dust species—especially silica—on circuit breaker performance, these studies primarily focused on isolated effects, neglecting the combined thermodynamic impact of multiple aerosol constituents. In reality, environmental dust often comprises a mixture of species, including Al_2O_3, CaO, Fe_2O_3, and CO, which can vary significantly depending on the geographical context. This study aims to assess the influence of such aerosols on the thermodynamic properties of air plasma under atmospheric pressure and local thermodynamic equilibrium conditions, across a temperature range of 2000 K to 30,000 K. The properties, including mass enthalpy, specific heat at constant pressure, sound velocity, and mass density, are computed directly from the population densities of the relevant species. Results reveal that the presence of aerosol mixtures alters the thermodynamic behaviour of the arc plasma during circuit interruption. Notably, reductions in mass enthalpy, specific heat, and sound velocity are observed with increasing temperature, while specific heat increases at temperatures below 7000 K. Additionally, mass density is found to increase with temperature. These findings suggest that aerosol contamination during the interruption phase can degrade circuit breaker performance, potentially resulting in residual leakage currents or fire risks due to incomplete arc quenching.

Keywords

Composition, Density, Enthalpy, Plasma, Heat, Sound, Aerosol

1. Introduction

Dust is an environmental factor that can accelerate the ageing and malfunction of electrical equipment. The West African region, situated within the intertropical zone, extends from 4˚N to the southern edge of the Sahara (~20˚N) and from 18˚W to 20˚E (eastern border of Lake Chad) [1]. This region is a significant source of desert aerosols, which include dust particles, sand, pollen, volcanic ash, and sea spray. The transport of these particles across West Africa is largely influenced by regional atmospheric dynamics, particularly the Harmattan and monsoon winds [1]-[4].

The chemical composition of aerosols in West Africa varies according to soil characteristics. Typically, they are composed of oxides of aluminium, calcium, iron, and silica (Al_2O_3, CaO, Fe_2O_3, and SiO_2, respectively) [5]-[12]. Desert aerosols often mix with urban pollutants like hydrocarbons [13] [14] and accumulate on electrical equipment, particularly circuit breakers. Through vent holes, the mixture enters circuit breakers and deposits on the electrodes and within the breaking chamber [15] [16]. **Figures 1-2** show dust episodes and accumulation on circuit breakers. Previous studies have demonstrated the impact of dust particles, such as silica, on circuit breaker performance. Silica significantly alters molar fractions, forming solid and liquid SiO_2 phases that condense on the gas generator surfaces. This process modifies the arc's dynamic viscosity and speed [15] [16]. Aerosols can degrade electrical circuits and components within circuit breakers. However, prior studies have not addressed the combined effects of various species, including Fe_2O_3, CaO, Al_2O_3, and CO, which may be present in dust deposits depending on regional conditions. This study aims to investigate the effects of aerosols on the thermodynamic properties of plasma in the West African region.

The remainder of this paper is organised as follows: Section 2 outlines the methods for computing thermodynamic properties; Section 3 discusses the effects of aerosols on these properties; and Section 4 presents the conclusions.

Figure 1. Dust storm in Niger in 2020 (https://sciencepost.fr).

Figure 2. Dust deposition on circuit breakers [15].

2. Methods and Materials

In West Africa, the period from February to April is characterised by large emissions of desert dust from the Saharan and local areas. However, the wet period from June to September and the period from December to January are characterised by small emissions of dust [17]. The most abundant chemical species in aerosols are silicon, calcium, iron, and aluminium oxides. The carbon oxide species are derived from biomass fires and fossil-fuel production. Further, silicon oxides account for up to 60% of the total mass. After silica, the most abundant oxides are aluminium (Al_2O_3) and ferric oxides (Fe_2O_3) [9] [10]. These proportions are directly linked to the texture of the soil itself. They're typically derived from analyses conducted in various studies across a sub-region. It's important to understand that these proportions are not static; they can vary significantly from one area to another due to differences in geology and topography. The composition and proportion of the chemical components of aerosols vary depending on the area. The mass proportions reflect desert sandstorms, regional soil composition, and human activity, with SiO_2 as the dominant species. The red colour of the dust in Ouagadougou indicates the presence of Fe_2O_3. Moreover, CaO has remarkable proportions, but less than Fe_2O_3 in Ouagadougou. The presence of Al_2O_3 is remarkable. We have not yet encountered work that establishes a clear composition of aerosols. Studies typically focus on mass fractions and specific chemical species based on the region [1] [3] [8]-[10].

A circuit breaker may need to operate in a polluted environment over a long duration. Our study found that aerosols were composed of silicon oxides, iron oxides, aluminium oxides, calcium oxides, and carbon monoxide. We assume that 1 g of aerosol contained the following mass percentages: 50% SiO_2, 20% Fe_2O_3, 10% Al_2O_3, 5% CO, and 15% CaO. This work is entirely theoretical because we do not have the equipment for experiments.

The mass fractions of the chemical elements of aerosol species that constitute the basic elements of the plasma were calculated using Equation (1) below:

$$\%A = \%air * \%A_{air} + \%aero \left(\begin{array}{l} \%A_k C_l \left(\frac{kM_A}{M_{A_k C_l}} \right) + \%A_x D_z \left(\frac{xM_A}{M_{A_x D_z}} \right) + \\ \%A_\gamma E_\beta \left(\frac{\gamma M_A}{M_{A_\gamma E_\beta}} \right) + \%A_\nu F_\theta \left(\frac{\nu M_A}{M_{A_\nu F_\theta}} \right) \end{array} \right) \quad (1)$$

where A, B, C, D, E, and F represent chemical elements; A_iB_j represents the chemical species of air of mass percentage %*air*; A_vF_θ, A_kC_l, A_xD_z, and $A_\gamma E_\beta$ represent the species brought by aerosols of mass percentage %*aero*; $M_{A_kC_l}$, $M_{A_xD_z}$, $M_{A_\gamma E_\beta}$, $M_{A_vF_\theta}$, M_A, M_B, M_C, and M_D represent the molar masses of the species considered; and i, j, k, l, x, z, θ, ν, β, and γ represent the numbers of atoms. From Equation (1), we obtain the mass percentages of the basic elements of our plasma, as listed in Table 1. The initial step in calculating the thermodynamic properties and transport coefficients is determining the equilibrium composition of the gas mixture using the principle of minimisation of the Gibbs free energy of the mixture [16] [18]-[21]. To this end, the specific chemical potential of all plasma particles must be determined [20]. Smoothed and tabulated thermodynamic data from Bonnie and Bendjebbar are used to calculate specific thermodynamic properties. The specific heat capacity, specific enthalpy, and specific entropy are obtained by Equation (2) [22] [23]:

$$\begin{cases} \dfrac{C_P^0(T)}{R} = a_1T^{-2} + a_2T^{-1} + a_3 + a_4T + a_5T^2 + a_6T^3 + a_7T^4 \\ \dfrac{H^0(T)}{RT} = -a_1T^{-2} + \mathrm{a}_2\dfrac{\ln(T)}{T} + a_3 + a_4\dfrac{T}{2} + a_5\dfrac{T^2}{3} + a_6\dfrac{T^3}{4} + a_7\dfrac{T^4}{5} + \dfrac{b_1}{T} \\ \dfrac{S^0(T)}{R} = -a_1\dfrac{T^{-2}}{2} + \mathrm{a}_2\dfrac{T^{-1}}{2} + a_3\ln(T) + a_4T + a_5\dfrac{T^2}{2} + a_6\dfrac{T^3}{3} + a_7\dfrac{T^4}{4} + b_2 \end{cases} \quad (2)$$

where R and T represent the constant of perfect gases and the temperature in Kelvin. The coefficients a_i and b_i for each particle are given by [22] [23].

For air-aerosol mixtures, 34 monatomic species have been considered (C, O, N, Si, Al, Fe, Ca, C^+, O^+, N^+, Si^+, Al^+, Fe^+, Ca^+, C^-, O^-, N^-, Si^-, Al^-, Fe^-, C^{++}, O^{++}, N^{++}, Si^{++}, Al^{++}, Fe^{++}, Ca^{++}, C^{+++}, O^{+++}, N^{+++}, Si^{+++}, Al^{+++}, Fe^{+++}, Ca^{+++}) and electrons; 31 diatomic species (C_2, O_2, N_2, Si_2, Al_2, Fe_2, Ca_2 CO, CN, SiC, AlC, NO, SiO, AlO, SiN, FeO, AlN, CaO, C_2^+, O_2^+, N_2^+, CO^+, CN^+, NO^+, AlO^+, CaO^+, N_2^-, C_2^-, O_2^-, CN^-, and AlO^-); and 40 polyatomic species (CO_2, C_3, CCN, CNC, CNN, C_2O, O_3, N_3, NCO, NO_2, N_2O, NCN, SiC_2, SiO_2, Si_2C, Si_2N, Si_3, AlC_2, AlO_2, Al_2O, OCCN, C_2N_2, CNCOCN, C_3O_2, C_4, NO_3, N_2O_3, N_2O_4, N_2O_5, Al_2C_2, Al_2O_2, Al_2O_3, $Fe(CO)_5$, N_2O^+, CO_2^+, Al_2O^+, $Al_2O_2^+$, AlO_2^-, NO_3^-, and NO_2^-).

In this study, the temperature range for the equilibrium composition was 2000 - 30000 K, assuming only the gaseous phase. Metals and their components are in solid form at low temperatures. At temperatures lower than approximately 2000 K, the plasma component can be established in air. The experiments are conducted at atmospheric pressure (1 bar), and therefore, all results of the thermodynamic properties are presented in this range.

2.1. Mass Density (kg/m^3)

Mass density is the quantity involved in the fluid mechanics equation. The density measures the amount of material contained in a given volume of plasma.

The following formula in Equation (3) was used [24].

$$\rho = \frac{P}{RT}\sum_{i=1}^{N} x_i M_i \tag{3}$$

where x_i, M_i, P, R, T, and N represent the molar fraction, molar mass of species i, pressure, molar gas constant, absolute temperature, and number of species in the plasma, respectively.

2.2. Mass Enthalpy (J/kg)

Mass enthalpy was calculated using the specific enthalpies of each particle and their molar fractions using x_i presented in Equation (4) [24] as:

$$h = \frac{1}{M}\left(\sum_{i=1}^{N} x_i \left(H_i^0 + H_f\right)\right) - \frac{k_b T}{6\pi\lambda_D^3} \tag{4}$$

where M represents the average molar mass, $M = \sum_{i=1}^{N} x_i M_i$ H_i^0 represents the molar enthalpy, and H_f represents the heat of formation at 298.15 K (J/mol) [23], and $k_b T/6\pi\lambda_D^3$ represents the Debye-Huckel term.

2.3. Specific Heat at Constant Pressure (J/kg/K)

The specific heat (C_p) is the amount of energy to be supplied by heat exchange to raise the temperature of a medium by 1˚. This indicated the ability of the system to store heat. If the thermodynamic transformation of the system is performed at constant pressure, the specific heat can be calculated and given by Equation (5) as [25].

$$C_p = \left(\frac{dh}{dT}\right) = \frac{h(T+\Delta T) - h(T)}{\Delta T} \tag{5}$$

where ΔT represents the variation in temperature ($\Delta T = 100K$), and T represents the temperature.

2.4. Velocity of Sound (m/s)

The velocity of sound was calculated using Equation (6) below [26]:

$$V_S = \left(\frac{RT}{M}\right)^{1/2} \tag{6}$$

Table 1. Mass percentage of the mixtures considered in this study.

%Air	%aerosol	%C	%O	%N	%Si	%Al	%Fe	%Ca
100	0	0	22.2	77.8	0	0	0	0
99	1	0.021	22.423	77.022	0.234	0.053	0.140	0.107
90	10	0.214	24.428	70.02	2.337	0.53	1.399	1.072
80	20	0.429	26.657	62.240	4.674	1.058	2.798	2.144
50	50	1.072	33.341	38.900	11.686	2.647	6.994	5.360
20	80	1.715	40.026	15.560	18.698	4.234	11.191	8.576

Table 2. Comparative analysis of the thermodynamic properties.

Temperature (K)	Mass density ($kg \cdot m^{-3}$)			Mass enthalpy ($J \cdot kg^{-1}$)			Specific heat ($Jkg^{-1} \cdot K^{-1}$)		
	Boulos	Result	Ecart (%)	Boulos	Result	Ecart (%)	Boulos	Result	Ecart (%)
7000	3.15E−2	3.22E−2	2.17	2.59E−7	2.60E−7	0.38	14,026	14,050.5	0.17
10000	1.72E−2	1.68E−2	2.38	4.84E−7	4.83E−7	0.21	4867.2	4761.62	2.22
15000	7.75E−3	7.78E−3	0.39	1.16E−8	1.11E−8	4.50	21,652	19,290.8	12.24
	D'Angola	Result	Ecart	D'Angola	Result	Ecart	D'Angola	Result	Ecart
7000	3.100E−2	3.223E−2	3.72	2.63E−7	2.60E−7	1.16	14,053.9	14,050.5	0.02
10000	1.69E−2	1.68E−2	0.59	4.87E−7	4.83E−7	0.83	4749.75	4761.62	0.25

3. Results and Discussions

3.1. Comparison

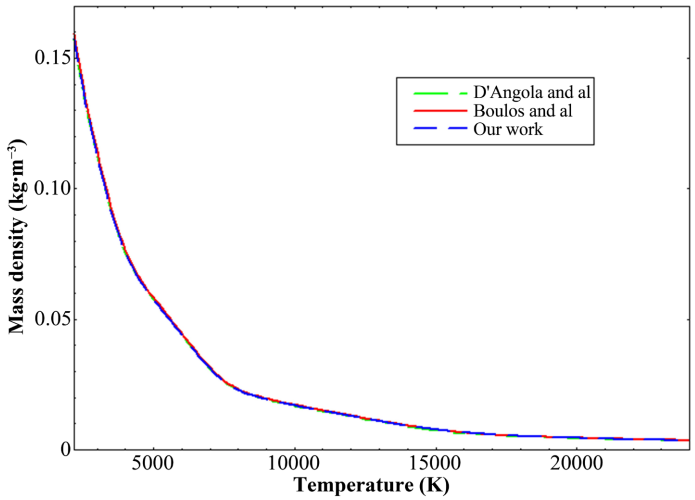

Figure 3. Comparison of mass density data of air plasma at atmospheric pressure.

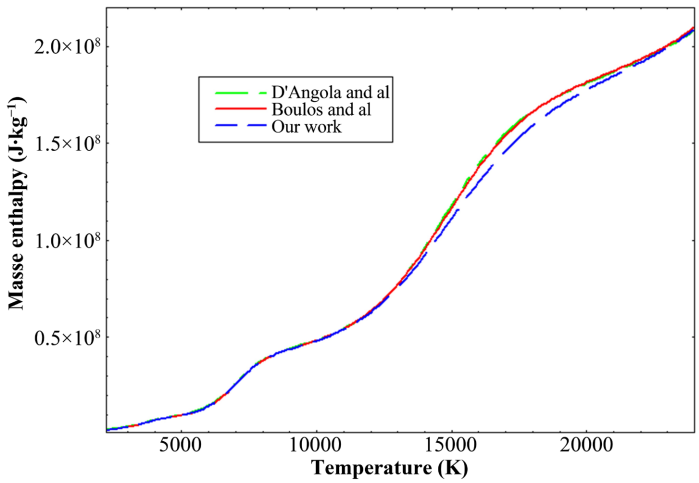

Figure 4. Comparison of mass enthalpy data of air plasma at atmospheric pressure.

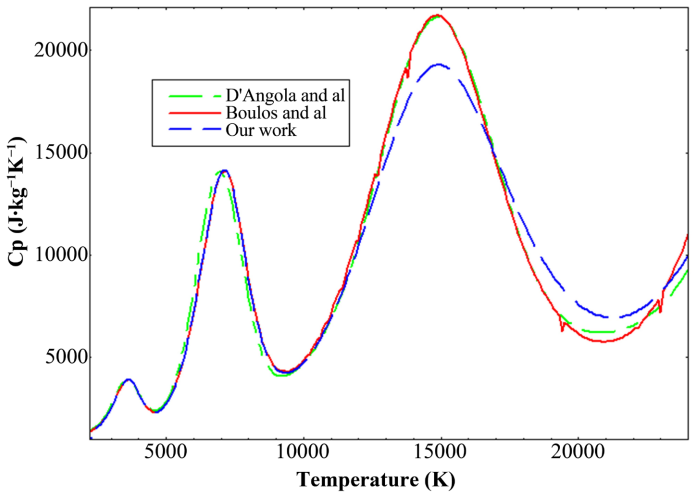

Figure 5. Comparison of specific heat data of air plasma at atmospheric pressure.

The thermodynamic of air-aerosol mixtures under the local thermodynamic equilibrium (L.T.E) assumption were evaluated across a temperature range of 2000 K - 30000 K at atmospheric pressure. These properties depend on the plasma composition, which is determined by minimising the Gibbs free energy. The local thermodynamic equilibrium is achieved when the rate of collisional processes is much higher than the rate of radiative processes (mainly radiative recombination and spontaneous emission).

No existing data were available for the exact mixture type studied here. However, previous research has examined various plasma models, including air, nitrogen, carbon dioxide (CO_2), CF_3I, argon-copper, argon-aluminium, C_4F_7N-CO_2-O_2, air-PA_{66}-copper, and C_4F_7N plasmas [27]-[38]. The MATLAB calculation method was validated by comparing its results with those from previous plasma studies. Thus, the properties of dry air plasma were compared with results from prior work to verify the data and equations used in these calculations [27]-[30]. The thermodynamic properties are presented in **Table 2**, where the mass density, mass enthalpy, and specific heat show satisfactory agreement with existing data, with an overall deviation of less than 7%. However, heat capacity showed a maximum deviation of 12.24% at 15,000 K compared to the data from Boulos *et al.* [27]. **Figures 3-5** show comparisons of the results for mass density, mass enthalpy, and heat capacity with the data from Boulos *et al.* [27] and D'Angola *et al.* [28]. The discrepancies observed can be attributed to the specific data used in this calculation program. Specific enthalpies, entropies, and chemical potentials were also calculated.

3.2. Effect of Aerosol Concentration on Thermodynamic Properties

Determining the chemical composition of plasma is essential for calculating thermodynamic properties. Previous studies have analysed the thermodynamic properties of various gas mixtures, including air [31] [32], CO_2 [33], SF_6 [34], and N_2 [35], and CF3I [33].

Figure 6 shows the mass densities of the air plasmas contaminated by aerosols. The evolution is identical for the different plasmas. The mass density decreases with increasing temperature; this decrease is greater at low temperatures (<8000 K). This is reflected by the decrease in the total density of species (rarefaction of the environment) imposed by the ideal gas law and by the presence of less massive species (atoms, ions and especially electrons) at high temperatures. These are direct consequences of the dissociation and ionisation of molecular and atomic species, which lead to the gradual disappearance of molecules and atoms with an increase in temperature [39]. The mass density of pure air coincided with the mass density of plasma containing 1% aerosols. Beyond 1%, the values of contaminated air plasmas are higher than those of pure air plasma; the more the plasma is contaminated, the higher is the increase in its mass density because they contain heavier particles than air. Table 3 lists the molar masses of the neutral species in the plasma.

Table 3. Molecular weight of neutral species [23].

Species	Molecular weight (g/mol)	Species	Molecular weight (g/mol)	Species	Molecular weight (g/mol)	Species	Molecular weight (g/mol)
C	12.01070	CO	28.01010	O_2	31.99880	SiN	42.09220
N	14.00670	CN	26.01740	N_2	28.01340	FeO	71.84440
O	15.99940	SiC	40.09620	Si_2	56.17100	AlN	40.98828
Si	28.08550	AlC	38.99224	Al_2	53.96308	CO_2	44.00950
Al	26.98154	NO	30.00610	Fe_2	111.6900	C_3	36.03210
Fe	55.84500	SiO	44.08490	C_2	24.02140	AlO	42.98094

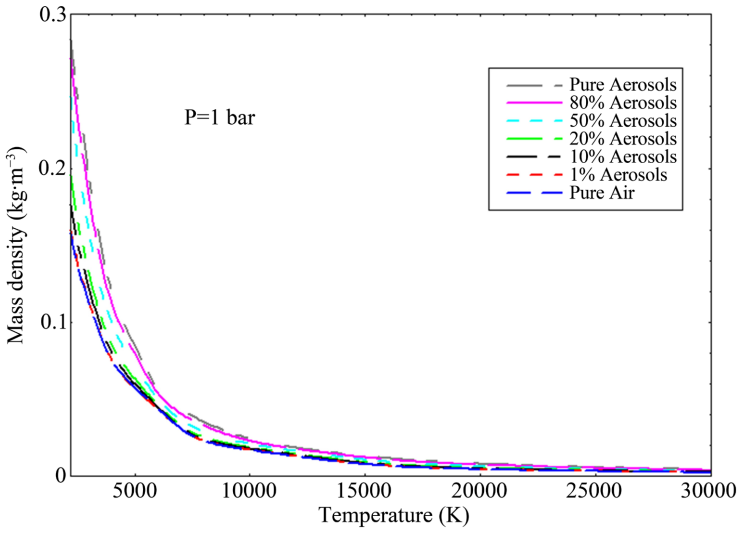

Figure 6. Evolution of the mass density of the plasma according to the percentage of aerosols, units: kg/m³.

The enthalpy curves (Figure 7) show rapid phases of evolution that correspond to the reactivity of the medium and to the dissociation and ionisation phenomena. Enthalpy varies inversely with mass density, and therefore, the enthalpy of the air plasma is greater than that of the polluted air plasma. In other words, the more polluted the air, the greater is the decrease in enthalpy.

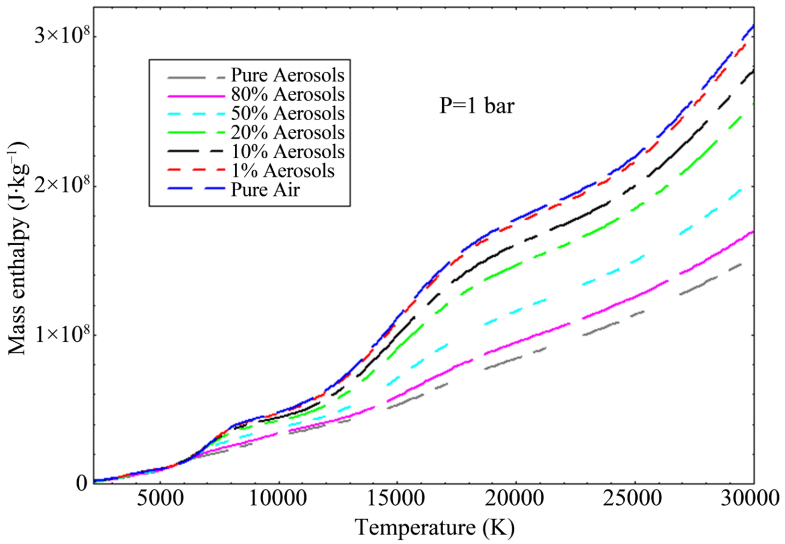

Figure 7. Evolution of the mass enthalpy of the plasma according to the percentage of aerosols, units: J/kg.

Figure 8 shows that specific heat strongly depends on the nature of the mixture and temperature, with the appearance of peaks in the regions where the enthalpy varies rapidly. The curves show the same pattern with the first peak at ~3500 K and the second at ~7000 K for up to 50% aerosols. Beyond this proportion, the peak gradually shifted towards lower temperatures (e.g. the peak was ~5500 K between 80% and 100% aerosols). The third peak occurs at ~15,000 K, where the peak moved slightly with an increase in the aerosol rate. These peaks represent the dissociation (of molecules) and ionisation (of atoms). The first peak (at ~3500 K) corresponds to the dissociation of CO_2, FeO, AlC, CN, SiC, AlC, SiN, NO, O_2, Al_2O, and SiO_3 molecules. For example, O_2, CO_2, and Al_2O dissociate at ~3500, 3400, and 4000 K [40]. Al_2 and Fe_2 dissociate below 3000 K [40], and C_3 and C_2 dissociate at ~5000 K [40]. The peak at ~5500 K for aerosols with mass percentages between 80% and 100% can be attributed to the dissociation of AlO and SiO. The dissociation peak of SiO appeared at ~5700 K at 1 atm [41].

The second peak corresponds to the dissociation of the CO and N_2 molecules. CO and N_2 dissociate at ~7000 K [40]. The first ionisation of the Al atom occurs at 9000 K [42] [43], whereas that of the Fe atom occurs between 8500 K and 9000 K [44]. Si and Ca ionise at the same temperature. The Al, Fe, Si, and Ca atoms ionise rapidly before the C, O, and N atoms because of their low ionisation energies ($Ei0_{Al}$ = 5.986 eV, $Ei0_{Ca}$ = 6.113 eV, $Ei0_{Fe}$ = 7.902 eV, $Ei0_{Si}$ = 8.151 eV, $Ei0_{C}$ = 11.26 eV, $Ei0_{O}$ = 13.628 eV, and $Ei0_{N}$ = 14.55 eV). The third peak corresponds to

the ionisation of C, O, and N atoms. The first ionisation of O and N is ~15,000 K [44].

The second ionisation of Al and Fe occurs around 19,000 K [42] [44]. The temperature corresponding to the second ionisation of C, O, and N was ~30,000 K [40] [44]. The first and second ionisations of Si and Ca were observed in the same temperature zones as iron and aluminium because of their similar ionisation energies. The effect of the aerosols was clear over the entire temperature range. Modifications to the locations of the main dissociation peaks are clearly observed. The movement of the peaks at low temperatures can be attributed to the chemistry. For example, for a 20% air-80% aerosol mixture, a peak was detected at ~5500 K, which can be attributed to the dissociation of AlO and SiO. Therefore, aerosols cause a decrease in specific heat because of the small energy ionisation of metals, except at temperatures below 7000 K. A high heat capacity means that the plasma can absorb more thermal energy for a given increase in temperature. This is beneficial for arc cooling, as a large portion of the arc's energy can be "stored" in the processes of dissociation and ionization rather than directly resulting in a temperature increase that would maintain the conductive plasma. These results show that the presence of aerosols leads to a slight increase in heat capacity. So a slight cooling of the plasma. The carbon released by the decomposition of CO can deposit as soot on insulating surfaces or contacts. These soot deposits can create undesirable conduction paths, leading to flashovers or a reduction in the dielectric strength of the insulators. In the presence of metallic vapors from the contacts, metallic carbides can form, also affecting the surfaces.

The presence of CO and its decomposition products can reduce the insulating capacity of the gaseous medium. Carbon particles can act as sites of electric field concentration, facilitating new discharges.

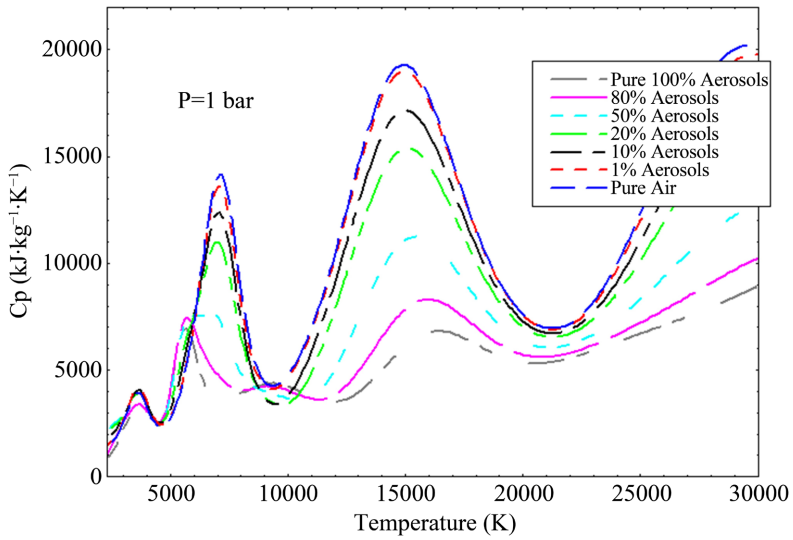

Figure 8. Evolution of the specific heat of the plasma according to the percentage of aerosols, units: J/kg/K.

Figure 9 shows the evolution of the sound velocity spread in air-aerosol plasmas, which decreases with the percentage of aerosols in the mixture. This decrease in sound propagation can be explained by heavy particles present in the polluted plasma. The higher the rate of contamination, the heavier is the plasma. This decreases the velocity.

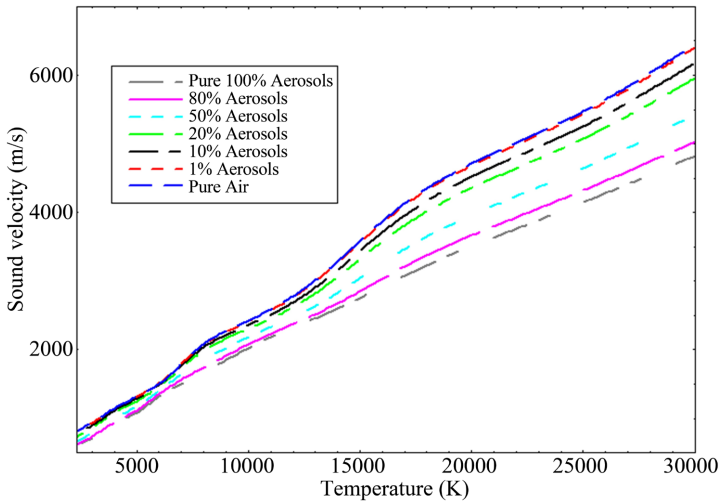

Figure 9. Evolution of the sound velocity of the plasma according to the percentage of aerosols, units: m/s.

4. Conclusions

This study examined the effect of aerosols on the thermodynamic properties of air plasma in a state of local thermodynamic equilibrium. Findings indicate that plasma density increases, whereas enthalpy, specific heat, and sound velocity all decrease, as the aerosol concentration in the mixture rises. Specific heat increased at temperatures below 7000 K and decreased at higher temperatures, with notable peaks at approximately 3500 K, 7000 K, and 15,000 K. Mass specific enthalpy is a key indicator of the arc plasma's energy state. Rapid reduction of this value is the fundamental goal of all arc extinction mechanisms in a circuit breaker to ensure reliable and safe current interruption. However, the presence of metal oxides can reduce the mass enthalpy and heat capacity at a given temperature. A potentially lower specific enthalpy and heat capacity would make arc quenching more difficult. The plasma remains conductive for longer, which extends the duration of the electric arc. A longer arc duration and sustained high temperatures increase the erosion of the circuit breaker's contacts, reducing their lifespan and potentially their reliability. In extreme cases, excessive oxide accumulation and unfavorable changes in plasma properties can lead to a failure to interrupt the circuit, with serious consequences for the electrical grid and equipment.

This theoretical analysis demonstrates that aerosols significantly impact plasma characteristics, including density, mass enthalpy, heat capacity, and sound velocity. Moreover, the plasma must be a good electrical insulator at low temperatures to facilitate the transient recovery voltage and to avoid restrikes.

While thermodynamic properties alone are insufficient to determine a circuit breaker's interruption capacity, they provide insight into the impact of aerosols on such capacity. Future studies should investigate the transport proprieties the dielectric strength properties, density variations, energy fluxes, and radiation effects, conducting experiments to comprehensively characterise plasma properties, including the influence of solid-phase aerosols.

Conflicts of Interest

The authors declare no conflicts of interest regarding the publication of this paper.

References

[1] Louvert, S. (2008) Modulations intrasaisonnières de la mousson d'Afrique de l'Ouest et impacts sur les vecteurs du paludisme à Ndiop (Sénégal): diagnostics et prévisibilité. Ph.D. Thesis, Université de Bourgogne (France).

[2] Legrand, M. (1990) Étude des aérosols sahariens au-dessus de l'Afrique à l'aide du canal à 10 microns de METEOSAT: Visualisation, interprétation et modélisation. Ph.D. Thesis, Université des Sciences et Techniques de Lille Flandres Artois (France).

[3] Malavelle, F. (2011) Effets direct et semi-direct des aérosols en Afrique de l'Ouest pendant la saison sèche. Ph.D. Thesis, Université Toulouse III Paul Sabatier (France).

[4] Pancrati, O. (2003) Analyse et modélisation des impacts des aérosols sahéliens sur le cycle hydrologique en Afrique de l'Ouest: Rôle des poussières et de la biomasse brûlée. Ph.D. Thesis, Université des Sciences et Technologies de Lille (France).

[5] Bouh, H.A., Benyaich, F., Bounakhla, M., Noack, Y., Tahri, M. and Zahry, F. (2013) Variations Saisonnières des particules atmosphériques et ses composants chimiques dans la Ville de Meknès-Maroc. *Journal of Materials and Environmental Science*, **4**, 49-62.

[6] Antenne, G.J.Y. (1985) Le phénomène des brumes sèches au Sénégal. Bulletin n7 de l'ORSTOM et du Centre de Météorologie Spatiale (Sénégal).

[7] Tobias, C. and Megie, C. (1980-1981) Les lithométéores au Tchad: Premiers résultats concernant la nature, la composition et l'importance des aérosols transportés par voie atmosphérique dans la région de N'Djamena (Tchad). *Office de la Recherche Scientifique et Technique Outre-Mer*, **18**, 71-81.

[8] Herrmann, L., Bleich, K.E., Sterk and Stahr, K. (310) Dépôt des poussières sur les sols en Afrique de l'Ouest: Propriétés et source des poussières et influence sur les propriétés des sols et sites. Year Université de Hohenheim, Institut pour la Science du sol et Ecologie.

[9] Orange, D. and Gac, J.Y. (1993) Geochemical Assessment of Atmospheric Deposition Including Harmattan Dust in Continental West Africa. Proc. IAHS.

[10] Orange, D. and Gac, J.Y. (1990) Bilan géochimique des apports atmosphériques en domaines sahélienne et sou-dano-guinéen d'Afrique de l'ouest (bassins supérieurs du Sénégal et de la Gambie). *Géodynamique*, **5**, 51-65.

[11] Doumbia, E.H.T. (2012) Caractérisation physico-chimique de la pollution atmosphérique en Afrique de l'Ouest et étude d'impact sur la santé. Ph.D. Thesis, Université Toulouse III-Paul Sabatier (France).

[12] Michaud, V. (2009) Modélisation et diagnostic de plasmas thermiques utilisés pour la coupure de l'arc électrique. Ph.D. Thesis, Université Blaise Pascal de Clermont-Ferrand (France).

[13] Flament, P., Deboudt, K., Cachier, H., Châtenet, B. and Mériaux, X. (2011) Mineral Dust and Carbonaceous Aerosols in West Africa: Source Assessment and Characterization. *Atmospheric Environment*, **45**, 3742-3749. https://doi.org/10.1016/j.atmosenv.2011.04.013

[14] Lemaître, C. (2011) Détermination du chauffage radiatif des aérosols désertiques au dessus de l'Afrique de l'Ouest et de leur impact sur la dynamique atmosphérique à l'aide d'observations satellitaires au cours de la campagne AMMA. Ph.D. Thesis, Université Paris VI.

[15] André, P., Courty, M.A., Kagoné, A.K., Koalaga, Z.K., Kohio, N.K. and Zougmoré, F. (2016) Calcul de la composition chimique dans un plasma issu de mélanges de PTFE, d'air, de cuivre et de vapeur d'eau dans le cadre d'appareillages de coupure électrique à air. *Journal International de Technologie, de l'Innovation, de la Physique, de l'Énergie et de l'Environnement*, **2**, 1.

[16] Yaguibou, W.C., Kohio, N., Kagoné, A.K., Koalaga, Z. and Zougmoré, F. (2018) Influence des aérosols sur la composition à l'équilibre d'un plasma d'air. J. Int. Technol. Innov. Phys. Energy Environ. *Journal International de Technologie, de l'Innovation, de la Physique, de l'Énergie et de l'Environnement*, **4**, 1.

[17] Bruno, K. (2014) Caractérisation optique et microphysique des aérosols atmosphériques en zone ur-baine ouest africaine: application aux calculs du forçage radiatif à Ouagadougou. Ph.D. Thesis, Université de Ouagadougou.

[18] André, P. (1995) Etude de la composition et des propriétés thermodynamiques des plasmas thermiques à l'équilibre et hors d'équilibre thermodynamique. Ph.D. Thesis, Université Blaise Pascal de Clermont-Ferrand II (France).

[19] Koalaga, Z. and André, P. (2010) Composition of a Thermal Plasma Formed from PTFE with Copper in Non-Oxidant Atmosphere. *High Temperature Material Processes: An International Quarterly of High-Technology Plasma Processes*, **14**, 295-303. https://doi.org/10.1615/HighTempMatProc.v14.i3.80

[20] Kohio, N., Kagone, A.K., Koalaga, Z. and Zougmore (2014) Thermodynamic Properties Calculation of Air-Water Vapor Mixtures Thermal Plasmas at Low Temperatures. *International Journal of Advanced Research in Science and Engineering Technology*, **1**, 240.

[21] Cayet, S. and Dudeck, M. (1996) Équilibre chimique dans des mélanges gazeux en déséquilibre thermique. *Journal de Physique III*, **6**, 403-420. https://doi.org/10.1051/jp3:1996130

[22] Bendjebbar, F., André, P., Benbakkar, M., Rochette, D., Flazi, S. and Vacher, D. (2012) Plasma Formed in Argon, Acid Nitric and Water Used in Industrial ICP Torches. *Plasma Science and Technology*, **14**, 683-692. https://doi.org/10.1088/1009-0630/14/8/01

[23] McBride, B.J., Zeche, M.J. and Gordon, S. (2002) Nasa Glenn Coefficients for Calculating Thermodynamic Properties of Individual Species. Glenn Research Center, 297.

[24] Berg, A.V.D. (2007) Measurement and Calculation of Thermodynamic Properties of Plasma in the Waste Pyrolysis Reactor. Ph.D. Thesis, Universiteit Gent Vakgroep Toegrpaste.

[25] Koalaga, Z. (1991) Contribution à l'étude expérimentale et théorique des plasmas d'arc laminés. Ph.D. Thesis, Université de Clermont Ferrand II (France).

[26] Gordon, S. and Mcbride, B.J. (1994) Computer Program for Calculation of Complex Chemical Equilibrium Compositions and Applications. NASA Reference Publication 1311, 58.

[27] Boulos, I.M., Fauchais, P. and Pfender, E. (1994) Thermal Plasmas: The Fundamentals and Applications. Plenum Press, 413-417.

[28] D'Angola, A., Colonna, G., Gorse, C. and Capitelli, M. (2007) Thermodynamic and Transport Properties in Equilibrium Air Plasmas in a Wide Pressure and Temperature Range. *The European Physical Journal D*, **46**, 129-150. https://doi.org/10.1140/epjd/e2007-00305-4

[29] Colonna, G., D'Angola, A., Laricchiuta, A., Bruno, D. and Capitelli, M. (2012) Analytical Expressions of Thermodynamic and Transport Properties of the Martian Atmosphere in a Wide Temperature and Pressure Range. *Plasma Chemistry and Plasma Processing*, **33**, 401-431. https://doi.org/10.1007/s11090-012-9418-4

[30] Capitelli, M., Colonna, G., Gorse, C. and D'Angola, A. (2000) Transport Properties of High Temperature Air in Local Thermodynamic Equilibrium. *The European Physical Journal D*, **11**, 279-289. https://doi.org/10.1007/s100530070094

[31] Cressault, Y., Hannachi, R., Teulet, P., Gleizes, A., Gonnet, J. and Battandier, J. (2008) Influence of Metallic Vapours on the Properties of Air Thermal Plasmas. *Plasma Sources Science and Technology*, **17**, Article ID: 035016. https://doi.org/10.1088/0963-0252/17/3/035016

[32] Tanaka, Y., Yokomizu, Y., Kato, M., Matsumura, T., Shimizu, K., Takayama, S. and Okada, T. (1996) Electrical and Thermal Conductivities and Enthalpy of Air Plasma Contaminated with Fe, Ca, Mg or H_2O Vapour. *Proceedings 4th International Conference on Plasma Processes*, Athens, 15-17 July 1996, 587.

[33] Yokomizu, Y., Ochiai, R. and Matsumura, T. (2009) Electrical and Thermal Conductivities of High-Temperature CO_2-CF_3I Mixture and Transient Conductance of Residual Arc during Its Extinction Process. *Journal of Physics D: Applied Physics*, **42**, Article ID: 215204. https://doi.org/10.1088/0022-3727/42/21/215204

[34] Colombo, V., Ghedini, E. and Sanibondi, P. (2008) Thermodynamic and Transport Properties in Non-Equilibrium Argon, Oxygen and Nitrogen Thermal Plasmas. *Progress in Nuclear Energy*, **50**, 921-933. https://doi.org/10.1016/j.pnucene.2008.06.002

[35] Chervy, B., Gleizes, A. and Razafinimanana, M. (1994) Thermodynamic Properties and Transport Coefficients in SF_6-Cu Mixtures at Temperatures of 300-30000 K and Pressures of 0.1-1 Mpa. *Journal of Physics D: Applied Physics*, **27**, 1193-1206. https://doi.org/10.1088/0022-3727/27/6/017

[36] Deng, J.W., Zhang, B.Y., Cao, M.C., *et al.* (2024) Radiation Properties of [C_4F_7N-CO_2-O_2]-PTFE-Cu Mixtures at High Temperatures and Pressures for High-Voltage Circuit Breakers. *Journal of Physics D: Applied Physics*, **58**, Article ID: 015206. https://doi.org/10.1088/1361-6463/ad809d

[37] Cressault, Y., Kimpeler, S., Moser, A. and Teulet, P. (2023) Thermophysical Properties of Air-Pa66-Copper Plasmas for Low-Voltage Direct Current Switches. *Plasma Physics and Technology*, **10**, 52-55. https://doi.org/10.14311/ppt.2023.1.52

[38] Zhong, L., Wang, J., Xu, J., Wang, X. and Rong, M. (2019) Effects of Buffer Gases on Plasma Properties and Arc Decaying Characteristics of C_4F_7N-N_2 and C_4F_7N-CO_2 Arc Plasmas. *Plasma Chemistry and Plasma Processing*, **39**, 1379-1396. https://doi.org/10.1007/s11090-019-10015-8

[39] Koalaga, Z., Abbaoui, M. and Lefort, A. (1993) Thermodynamic Properties Calculation of $C_{alpha}H_{beta}O_{gamma}N_{theta}$ Insulator Plasmas. *Journal of Physics D: Applied Physics*, **26**, 393-403. https://doi.org/10.1088/0022-3727/26/3/008

[40] Cressault, Y., Connord, V., Hingana, H., Teulet, P. and Gleizes, A. (2011) Transport Properties of CF_3I Thermal Plasmas Mixed with CO_2, Air or N_2 as an Alternative to SF_6 Plasmas in High-Voltage Circuit Breakers. *Journal of Physics D*: *Applied Physics*, **44**, Article ID: 495202. https://doi.org/10.1088/0022-3727/44/49/495202

[41] André, P., Bussière, W. and Rochette, D. (2007) Transport Coefficients of Ag-SiO_2 Plasmas. *Plasma Chemistry and Plasma Processing*, **27**, 381-403. https://doi.org/10.1007/s11090-007-9086-y

[42] Wang, W., Rong, M., Wu, Y. and Yan, J.D. (2012) Thermodynamic and Transport Properties of Two-Temperature SF_6 Plasmas. *Physics of Plasmas*, **45**, Article ID: 083506. https://doi.org/10.1063/1.4739778

[43] Liu, Y., Wang, X., Zhong, L., Yang, A., Rong, M. and Wu, J. (2018) Influence of Al, Fe or Cu Vapour on Thermophysical Properties of CO_2 Plasmas. *The European Physical Journal D*, **72**, Article No. 215. https://doi.org/10.1140/epjd/e2018-80591-3

[44] Cressault, Y., Murphy, A.B., Teulet, P., Gleizes, A. and Schnick, M. (2013) Thermal Plasma Properties for Ar-Cu, Ar-Fe and Ar-Al Mixtures Used in Welding Plasmas Processes: II. Transport Coefficients at Atmospheric Pressure. *Journal of Physics D*: *Applied Physics*, **46**, Article ID: 415207. https://doi.org/10.1088/0022-3727/46/41/415207